

Low-temperature Quantum Metrology Enhanced by Strong Couplings

Ze-Zhou Zhang,¹ Hong-Gang Luo,¹ and Wei Wu^{1,*}

¹*Key Laboratory of Quantum Theory and Applications of Ministry of Education,
Lanzhou Center for Theoretical Physics and Key Laboratory of Theoretical
Physics of Gansu Province, Lanzhou University, Lanzhou 730000, China*

Equilibrium probes have been widely used in various noisy quantum metrology schemes. However, such an equilibrium-probe-based metrology scenario severely suffers from the low-temperature-error-divergence problem in the weak-coupling regime. To circumvent this limit, we propose a strategy to eliminate the error-divergence problem by utilizing the strong coupling effects, which can be captured by the reaction-coordinate mapping. The strong couplings induce a noncanonical equilibrium state and greatly enhance the metrology performance. It is found that our metrology precision behaves as a polynomial-type scaling relation, which suggests the reduction of temperature can be used as a resource to improve the metrology performance. Our result is sharply contrary to that of the weak-coupling case, in which the metrology precision exponentially decays as the temperature decreases. Paving a way to realize a high-precision noisy quantum metrology at low temperatures, our result reveals the importance of the non-Markovianity in quantum technologies.

Introduction.— Quantum metrology is a rapidly developing research field, which aims at surpassing the precision limit set by classical statistics [1–3]. It has been widely demonstrated that some quantum resources, such as quantum entanglement [4–6] and quantum squeezing [7–9], are able to boost the metrology performance for the noiseless ideal case. However, in any practical metrology scenarios, the probe, in which the parameter of interest is intrinsic or externally imprinted, inevitably interacts with its surrounding bath [10–14]. Thus, the effect of decoherence should be taken into account. Roughly speaking, there are two kinds of quantum probe used in the studies of noisy quantum metrology: one is the equilibrium probe [15–19] and the other one is the nonequilibrium dynamical probe [20–23]. If the decoherence time is shorter than the probe-bath interaction time, the probe is fully thermalized. In this case, the signal-to-noise ratio (SNR) of the estimated parameter is obtained from the equilibrium state of the probe. If the interaction time is very short, the coherence can be partially reserved, and the SNR is then read out from dynamical signals.

Compared with the nonequilibrium dynamical probe, the equilibrium one has certain advantages. For example, the equilibrium-probe scheme does not require any precise dynamical control to find the optimal interrogation time [24–27] and is commonly universal to different initial states. However, except for very a few solvable models, an analytical expression for the probe’s equilibrium state is generally difficult to be obtained. The utilization of numerical tools may be a possible solution [28–30], but it relies heavily on computing resources. The other way to overcome this restriction is the employment of the weak-coupling approximation, which assumes the coupling between the probe and the bath is so weak that the probe experiences a canonical thermalization. Under this approximate framework, the equilibrium state of the probe can be described by a canonical equilibrium (Gibbs) state, which greatly simplifies the difficulties in calcu-

lating the SNR. Unfortunately, the weak-coupling approximation neglects the system-bath correlations, which is commonly viewed as a non-Markovian effect [31–33]. This treatment gives rise to a divergent metrology error at low temperature, which has been pointed out in various quantum thermometries [15, 18, 34–37] and the quantum metrology for Hamiltonian parameters [19, 38–41]. It is highly desirable to develop an alternative scheme to eliminate this problem.

In this Letter, we propose a strategy to improve the precision of an equilibrium-probe-based noisy frequency estimation scenario via strong couplings. By using the reaction-coordinate mapping [33, 42–44], in the strong-coupling regime, we find the noncanonical characteristics occurs in the equilibrium state of the probe that are composed of N spin-1/2 particles. Such a noncanonicity is induced by the non-Markovianity [32, 33, 43, 45–48], which is neglected in the usual weak-coupling treatment. At low temperatures, it is found that the SNR from our strategy can maintain as a temperature-independent constant or behave as a polynomial scaling relation according to different spin numbers. This result is sharply contrary to that of the weak-coupling case, in which the SNR exponentially decays when the temperature is lowered, and completely remove the error-divergence problem.

Weak-coupling approximation.— In this Letter, we consider a quantum metrology scenario of noisy frequency estimation, which is experimentally related to the atomic spectroscopy [20, 49, 50]. In our task, we estimate the frequency of a quantum probe, which is composed of multiple spin-1/2 particles with the Hamiltonian $\hat{H}_s = \epsilon \hat{J}_z$. Here, ϵ is the parameter to be determined and $\hat{J}_v \equiv \frac{1}{2} \sum_{n=1}^N \hat{\sigma}_n^v$ with $v = x, y, z$ are the collective spin operators. Such an estimation of ϵ can be realized via a unitary dynamics in the ideal noiseless case [11]. However, such a unitary metrology scheme breaks down when the inevitable noises from the surrounding environment are taken into account. In the noisy metrological case,

we assume the influences of environmental noises can be described via a linear interaction between the probe and a thermal bosonic bath $\hat{H}_b = \sum_k \omega_k \hat{b}_k^\dagger \hat{b}_k$, which is in a thermal equilibrium at the temperature $T = 1/\beta$ ($k_B = 1$). The total Hamiltonian reads ($\hbar = 1$)

$$\hat{H} = \hat{H}_s + \hat{H}_b + \hat{J}_x \sum_k g_k (\hat{b}_k^\dagger + \hat{b}_k), \quad (1)$$

where \hat{b}_k and \hat{b}_k^\dagger are the annihilation and creation operators of the k th bosonic mode with frequency ω_k , respectively. Parameters g_k denote the coupling strength between the probe and the k th bosonic mode. The frequency dependence of the interaction strengths is encoded into the spectral density $J(\varpi) \equiv \sum_k g_k^2 \delta(\varpi - \omega_k)$. The explicit expression of $J(\varpi)$ will not be addressed here, because our result is universal to the form of $J(\varpi)$ [44].

Assuming the probe-bath interaction time is sufficiently long, the probe shall evolve to its long-time steady state. This equilibrium state is approximated as a Gibbs state $\rho_s^{\text{weak}}(\infty) = e^{-\beta \hat{H}_s} / Z$ with $Z \equiv \text{Tr}(e^{-\beta \hat{H}_s})$, if one takes the weak-coupling approximation [48, 51–53]. Under this approximation, by measuring the observable \hat{J}_z , one can easily find the SNR $\mathbb{S} = |\partial_\epsilon \langle \hat{J}_z \rangle|^2 / (\langle \hat{J}_z^2 \rangle - \langle \hat{J}_z \rangle^2)$ is given by

$$\mathbb{S}_{\text{weak}} = \frac{N\beta^2}{2 + 2 \cosh(\beta\epsilon)}. \quad (2)$$

From the above expression, one proves that

$$\lim_{T \rightarrow 0} \mathbb{S}_{\text{weak}} \propto e^{-\epsilon/T}, \quad (3)$$

which means the SNR of the equilibrium-state probe exponentially decay as $\epsilon/T \rightarrow 0$. This is the outstanding error-divergence problem [15, 18, 19, 34–41], which severely limits the equilibrium-probe-based quantum metrology at low temperature.

To overcome the above problem, one needs to go beyond the limitation of the weak-coupling approximation, because a strong probe-bath coupling is able to induce the non-Markovian and the bound-state effects, which are beneficial to improve the metrology performance [13, 21, 22, 54, 55]. However, the exactly analytical expression for the equilibrium state of the probe is general difficult to obtain. Fortunately, as demonstrated in many previous studies [33, 43, 56–58], the long-time behaviour of a quantum dissipative dynamics can be faithfully captured by the reaction-coordinate-mapping approach, which provides a simple but accurate expression to describe the probe's equilibrium state when suitable parameters in the spectral density are chosen. Next, we apply this technique to our metrology scenario.

Reaction-coordinate-mapping approach.—The reaction coordinate transformation, which is an orthogonal transformation, maps the original Hamiltonian \hat{H} to a dynamically equivalent Hamiltonian $\hat{\mathcal{H}}$ [59]. As displaced

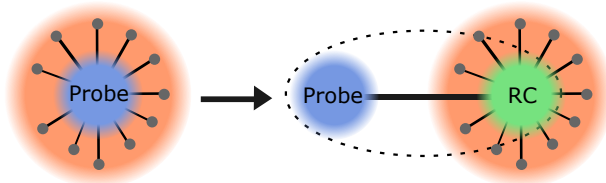


FIG. 1. Diagrammatic sketch of the reaction-coordinate mapping. In the original Hamiltonian, a quantum probe with Hamiltonian \hat{H}_s , which is large spin system, is directly coupled to a thermal bosonic bath. By applying the reaction-coordinate mapping, the probe interacts with a RC mode within an extend composite system with Hamiltonian $\hat{\mathcal{H}}_s$, which is in turn weakly connected to a residual thermal bath. In the reaction-coordinate-mapping picture, the equilibrium of the probe is corrected as a noncanonical state $\rho_s(\infty) \propto \text{Tr}_{\text{RC}}[\exp(-\beta \hat{\mathcal{H}}_s)]$, compared with the weak-coupling result $\rho_s^{\text{weak}}(\infty) \propto \exp(-\beta \hat{H}_s)$.

in Fig. 1, in the picture of the reaction-coordinate mapping, the probe is directly interacts with one collective reaction coordinate (RC) mode, which is in turn coupled to a residual environment. The mapped Hamiltonian reads $\hat{\mathcal{H}} = \hat{\mathcal{H}}_s + \hat{\mathcal{H}}_b + \hat{\mathcal{H}}_{\text{int}} + \hat{\mathcal{H}}_c$, where

$$\hat{\mathcal{H}}_s = \hat{H}_s + \omega \hat{a}^\dagger \hat{a} + g \hat{J}_x (\hat{a}^\dagger + \hat{a}). \quad (4)$$

Here, the coupling strength g and the frequency of the RC mode ω are given in terms of $J(\varpi)$ [17, 56]. The residual environment reads $\hat{\mathcal{H}}_b = \sum_k \tilde{\omega}_k \hat{a}_k^\dagger \hat{a}_k$, $\hat{\mathcal{H}}_{\text{int}} = (\hat{a}^\dagger + \hat{a}) \sum_k \tilde{g}_k (\hat{a}_k^\dagger + \hat{a}_k)$ is the interaction Hamiltonian and $\hat{\mathcal{H}}_c = (\hat{a}^\dagger + \hat{a})^2 \sum_k \tilde{g}_k^2 / \tilde{\omega}_k$ is the counterterm.

Through this approach, the probe \hat{H}_s is incorporated within an extend composite system $\hat{\mathcal{H}}_s$. One can realize an arbitrarily strong probe-bath coupling in the original Hamiltonian \hat{H} , while having arbitrarily small coupling between $\hat{\mathcal{H}}_s$ and $\hat{\mathcal{H}}_b$ in the mapped one [59]. Under this condition, one finds the long-time steady state of the composite system is well-described by $\varrho_s(\infty) = e^{-\beta \hat{\mathcal{H}}_s} / \mathcal{Z}$ with $\mathcal{Z} = \text{Tr}(e^{-\beta \hat{\mathcal{H}}_s})$. After tracing out the RC degrees of freedom, the steady state for the probe can be obtained accordingly as $\rho_s(\infty) = \text{Tr}_{\text{RC}}[\varrho_s(\infty)]$. The validity for the noncanonical state of $\rho_s(\infty)$ has been demonstrated via some numerically rigorous methods in Refs. [33, 43, 56, 57]. Compared with the weak-coupling case, the phenomenon of the noncanonical equilibration is captured by the reaction-coordinate-mapping treatment, which faithfully reflects the probe-bath correlations or the non-Markovian effects in strong-coupling regimes.

With the expression of $\rho_s(\infty)$ at hand, the SNR can be easily obtained via numerically diagonalizing $\hat{\mathcal{H}}_s$. To make a comparison and to build a clear physical picture, we also provide an analytical result from the generalized rotating-wave approximation (GRWA) [60–63]. Good agreement is found (see the comparisons in Supplemental Materials [59]).

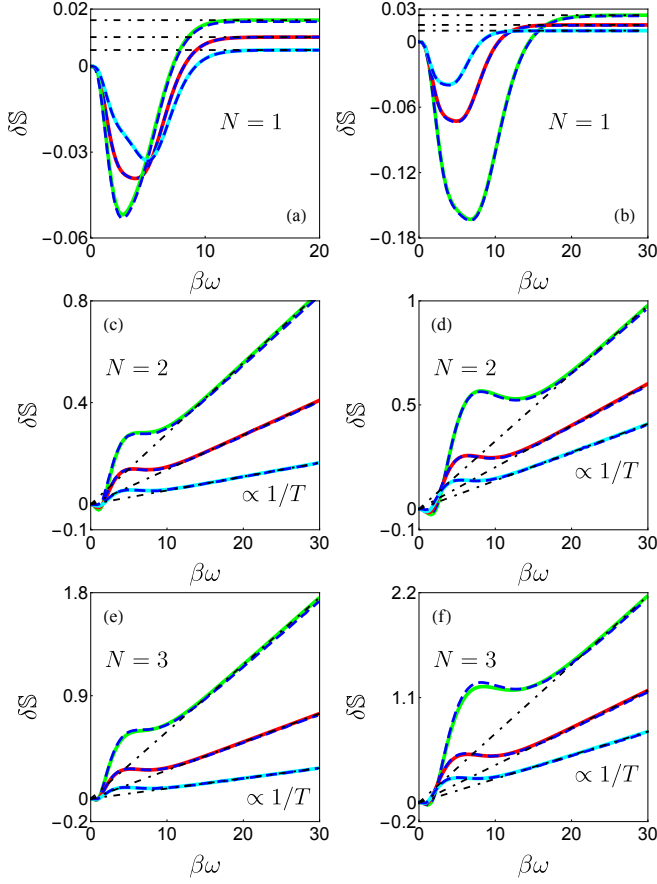


FIG. 2. Left panel: $\delta\mathbb{S}$ versus $\beta\omega$ with $\epsilon = \omega$ for different parameters $(g/\omega, N) = (0.3, 1)$ (cyan line), $(g/\omega, N) = (0.4, 1)$ (red line) and $(g/\omega, N) = (0.5, 1)$ (green line) in (a); $(g/\omega, N) = (0.2, 2)$ (cyan line), $(g/\omega, N) = (0.3, 2)$ (red line) and $(g/\omega, N) = (0.4, 2)$ (green line) in (c), and $(g/\omega, N) = (0.2, 3)$ (cyan line), $(g/\omega, N) = (0.3, 3)$ (red line) and $(g/\omega, N) = (0.4, 3)$ (green line) in (e). Right panel: $\delta\mathbb{S}$ versus $\beta\omega$ for $\epsilon/\omega = 1$ (cyan line), $\epsilon/\omega = 0.8$ (red line) and $\epsilon/\omega = 0.6$ (green line) with $g/\omega = 0.4$ and $N = 1$ in (b); $g/\omega = 0.3$ and $N = 2$ in (d); $g/\omega = 0.3$ and $N = 3$ in (f). The blue dashed lines are analytical results predicted by the GRWA method, while the black dot-dashed lines are approximate results from Eq. (7) and Eq. (8) with E_g from the GRWA approach.

Generalized rotating-wave approximation.—In the GRWA treatment, we first apply a unitary transformation to $\hat{\mathcal{H}}_s$ as $\hat{\mathcal{H}}'_s = e^{\lambda\hat{J}_x(\hat{a}^\dagger - \hat{a})}\hat{\mathcal{H}}_s e^{-\lambda\hat{J}_x(\hat{a}^\dagger - \hat{a})}$ with λ being self-consistently determined by minimizing the ground-state energy. The transformed Hamiltonian is

$$\hat{\mathcal{H}}'_s = (\omega\lambda^2 - 2g\lambda)\hat{J}_x^2 + \omega\hat{a}^\dagger\hat{a} + (g - \omega\lambda)J_x(\hat{a}^\dagger + \hat{a}) + \epsilon\hat{J}_z \cosh[\lambda(\hat{a}^\dagger - \hat{a})] - i\hat{J}_y \sinh[\lambda(\hat{a}^\dagger - \hat{a})]. \quad (5)$$

Neglect all the higher-order contributions, an effective

Hamiltonian can be obtained [59]

$$\hat{\mathcal{H}}_s^{\text{GRWA}} = \tilde{\epsilon}\hat{J}_z + \Delta\hat{J}_x^2 + \omega\hat{a}^\dagger\hat{a} + \frac{1}{2}\tilde{g}(\hat{J}_-\hat{a}^\dagger + \hat{J}_+\hat{a}) + \frac{1}{2}\epsilon\left[\hat{J}_-\hat{a}^\dagger F_1(\hat{a}^\dagger\hat{a}) + \hat{J}_+ F_1(\hat{a}^\dagger\hat{a})\hat{a}\right], \quad (6)$$

where $\hat{J}_\pm \equiv \hat{J}_x \pm i\hat{J}_y$, $\tilde{\epsilon} = \epsilon F_0(\hat{a}^\dagger\hat{a})$ is the renormalized frequency, $\Delta = \omega\lambda^2 - 2g\lambda$ and $\tilde{g} = g - \lambda\omega$. Here, $F_n(m) \equiv \frac{m!}{(m+n)!} e^{-\frac{1}{2}\lambda^2} \lambda^n L_m^n(\lambda^2)$ with $L_m^n(\lambda^2)$ being the Laguerre polynomials. Note that $\hat{\mathcal{H}}_s^{\text{GRWA}}$ is a block-diagonal matrix in the product basis, one can diagonalize it by hand, and the corresponding SNR can be analytically obtained. Next, we use several examples to illustrate the advantages of the strong coupling on the low-temperature frequency estimation with a Lorentzian spectral density [59].

Quantum Rabi model case.—For the finite- N cases, $\hat{\mathcal{H}}_s$ is the famous quantum Rabi model [64–66]. In Fig. 2 (a) and (b), we display $\delta\mathbb{S} \equiv \mathbb{S} - \mathbb{S}_{\text{weak}}$ as a function of the temperature with $N = 1$. As long as $\delta\mathbb{S} > 0$, one concludes the strong coupling improves the metrology performance. Sharply contrary to the exponentially-decay behaviour in the weak-coupling case, we find $\mathbb{S}_{N=1}$ remains as a constant when the temperature approaches to zero. This result can be well-explained as follows. When $(E_e - E_g)/E_g \ll 1$ with E_e being the first excited energy, one can neglect the contributions from the high-energy eigenstates and reexpressed the partition function as $\mathcal{Z} \simeq \exp(-\beta E_g)$. This result leads to

$$\lim_{T \rightarrow 0} \mathbb{S}_{N=1} \propto \frac{4(\partial_\epsilon^2 E_g)^2}{1 - 4(\partial_\epsilon E_g)^2}, \quad (7)$$

which is independent of the temperature. The above low-temperature asymptotic result is confirmed by both the GRWA approach and the exact diagonalization method as displayed in Fig. 2 (a) and (b).

The quantum Rabi model with $N = 1$ can be experimentally simulated by means of the superconducting circuit, which allows the realization of strong and ultra-strong couplings. Using the experimentally available parameters in Ref. [67], we find $\mathbb{S}_{N=1}/\mathbb{S}_{\text{weak}} \simeq 936$ with $\epsilon/2\pi = 3.84$ GHz, $\omega/2\pi = 5.588$ GHz, $g/2\pi = 5.63$ GHz and $T = 45$ mK. One sees that $\mathbb{S}_{N=1}$ is larger by almost 3 orders of magnitude than \mathbb{S}_{weak} , which evidently demonstrates the enhancement effect of strong couplings.

For the cases of $N = 2$ and $N = 3$, we find

$$\lim_{T \rightarrow 0} \mathbb{S}_{N \geq 2} \propto -\frac{1}{T} \partial_\epsilon^2 E_g. \quad (8)$$

Note that $\partial_\epsilon^2 E_g < 0$ [59], this result suggests a T^{-1} scaling behaviour in low-temperature regimes. Such a scaling relation is confirmed by both the analytical and the numerical methods as displayed in Fig. 2 (c)-(f). This surprised result means the metrological precision can be

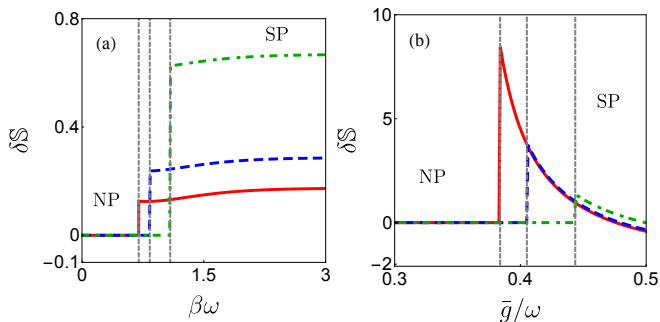


FIG. 3. (a) The modified SNR $\delta\mathcal{S} \equiv (\mathbb{S}_{\text{DM}} - \mathbb{S}_{\text{weak}})/N$ in the Dicke model case versus $\beta\omega$ with $\epsilon = 3\omega$ for different coupling strengths: $\bar{g}/\omega = 0.98$ (red solid line), $\bar{g}/\omega = 0.94$ (blue dashed line) and $\bar{g}/\omega = 0.9$ (green dot-dashed line). (b) $\delta\mathcal{S}$ versus \bar{g}/ω with $\epsilon = 0.5\omega$ for different $\beta\omega$: $\beta\omega = 5$ (red solid line), $\beta\omega = 4$ (blue dashed line) and $\beta\omega = 3$ (green dot-dashed line). The gray dotted lines separate the boundaries of the normal phase and the superradiant phase.

increased by decreasing the temperature in our strategy, which is quite similar to the Landau-bound-type scaling relation in the studies of temperature sensing [15, 68]. Moreover, we find that the T^{-1} -scaling relation seems universal for all the finite- N cases [59]. This universality greatly expands the general applicability of our proposed scheme. All these results prove the error-divergence problem in the noisy frequency metrology can be completely eliminated by strong couplings. Next, we generalize our analysis to the limit of $N \rightarrow \infty$.

Dicke model case.—In the limit of $N \rightarrow \infty$, $\hat{\mathcal{H}}_s$ becomes the famous quantum Dicke model [69], whose thermodynamic properties has been widely discussed in previous studies [70–73]. In this large- N case, the excitation spectrum of the Dicke model becomes quasicontinuous, namely, the energy gap between the ground state and the first excited state becomes infinitesimal (almost gapless), which breaks down the condition $(E_e - E_g)/E_g \ll 1$. Thus, neither the conclusions nor the methodology used in the finite- N cases is directly applicable to the present situation. Fortunately, as displayed in Refs. [70–73], the Dicke model is exactly solvable in the limit $N \rightarrow \infty$. Via computing its partition function, the corresponding SNR can be analytically derived.

Following Refs. [70–73], the partition function of the Dicke model is given by [59]

$$\mathcal{Z}_{\text{DM}} = \sqrt{\frac{2}{\beta\omega|\partial_z^2\Phi(z)|}} e^{N\Phi(z)} \Big|_{z=z_0}, \quad (9)$$

where $\Phi(z) = -\beta z^2 + \ln[2 \cosh(\frac{1}{2}\beta\sqrt{\epsilon^2 + 16\bar{g}^2 z^2})]$ with $\bar{g} = \sqrt{N}g/2$ and z_0 being determined by the equation $\partial_z\Phi(z)|_{z=z_0} = 0$. There are two possible roots for

$\partial_z\Phi(z)|_{z=z_0} = 0$, depending on the critical temperature

$$T_c^{\text{DM}} = \epsilon \left[2 \operatorname{arctanh} \left(\frac{\epsilon\omega}{4\bar{g}^2} \right) \right]^{-1} \quad (10)$$

at which the Dicke model experiences a thermodynamic phase transition. When $T > T_c^{\text{DM}}$, the Dicke model is in the normal phase with a trivial solution $z_0 = 0$ corresponding to the case in which the spins and the RC mode are completely decoupled. On the other hand, if $T \leq T_c^{\text{DM}}$, the Dicke model is in the superradiant phase with a nontrivial solution $z_0 = \sqrt{\epsilon^2\eta^2 - \epsilon^2}/(4\bar{g})$ where η is determined by $\frac{1}{4}\eta\epsilon\omega\bar{g}^{-2} = \tanh(\frac{1}{2}\beta\eta\epsilon)$ [70, 71].

With the above thermodynamic properties at hand, we find the SNR in the Dicke mode case is given by [59]

$$\frac{\mathbb{S}_{\text{DM}}}{N} = \begin{cases} \beta^2/[2 + 2 \cosh(\beta\epsilon)], & T > T_c^{\text{DM}}, \\ \omega^2/(16\bar{g}^4 - \epsilon^2\omega^2), & T \leq T_c^{\text{DM}}. \end{cases} \quad (11)$$

From the above expression, one sees \mathbb{S}_{DM} in the normal phase has the same expression with that of the weak-coupling case, which means \mathbb{S}_{DM} still suffers from the error-divergence problem at low temperatures. However, in the superradiant phase, the SNR becomes independent of the temperature circumventing the error-divergence problem. By engineering the parameters $\{\epsilon, \omega, \bar{g}\}$, the value of the SNR in the superradiant phase can be larger than \mathbb{S}_{weak} , as plotted in Fig. 3. Though the result of $\mathbb{S}_{\text{DM}} \propto T^0$ in the superradiant phase is similar to the case of Rabi model with $N = 1$, these results are generated by different physical mechanisms. Moreover, when crossing over the phase boundary, one sees \mathbb{S}_{DM}/N exhibits a discontinuous behavior resulting in a local maximum SNR at the phase transition point. Such a singularity is quite similar to previous studies of quantum critical metrology at zero temperature [74–80] and can be used to reveal the thermal phase transition without a prior knowledge about the order parameter or the symmetry. Our result suggests a phase transition, even happens at finite temperature, can be used as a resource to increase the metrology performance, which provides a possibility of realizing a quantum critical metrology without cooling down to $T \simeq 0$ K.

Conclusion.—In summary, we show that the error-divergence problem in a noisy frequency estimation task at low-temperature stems from the unnecessary weak-coupling approximation, which leads to a canonical thermalization for the probe within the Born-Markovian treatment. By employing the reaction-coordinate mapping, we overcome the restrict of the weak-coupling approximation and are able to study the influences of strong coupling, which naturally generates a noncanonical equilibrium state for the probe, on the metrology performance. By considering the strong-coupling effect, it is found that the SNR displays as a T^θ -type scaling relation with $\theta = 0$ for $N = 1, \infty$; and $\theta = -1$ for

other finite- N cases. This result is sharply contrary to the exponentially-decay SNR in the weak-coupling case. In this sense, we completely remove the error-divergence problem by the strong couplings. Paving a way to realize a high-precision quantum metrology at low temperature, our result reveals the importance of a proper understanding of equilibrium states in quantum technologies.

Acknowledgments.—This work is supported by the National Natural Science Foundation of China (Grants No. 12375015, and No. 12247101).

* wuw@lzu.edu.cn

- [1] Luca Pezzè, Augusto Smerzi, Markus K. Oberthaler, Roman Schmied, and Philipp Treutlein, “Quantum metrology with nonclassical states of atomic ensembles,” *Rev. Mod. Phys.* **90**, 035005 (2018).
- [2] C. L. Degen, F. Reinhard, and P. Cappellaro, “Quantum sensing,” *Rev. Mod. Phys.* **89**, 035002 (2017).
- [3] John F. Barry, Jennifer M. Schloss, Erik Bauch, Matthew J. Turner, Connor A. Hart, Linh M. Pham, and Ronald L. Walsworth, “Sensitivity optimization for nv -diamond magnetometry,” *Rev. Mod. Phys.* **92**, 015004 (2020).
- [4] Dany Lachance-Quirion, Samuel Piotr Wolski, Yutaka Tabuchi, Shingo Kono, Koji Usami, and Yasunobu Nakamura, “Entanglement-based single-shot detection of a single magnon with a superconducting qubit,” *Science* **367**, 425–428 (2020).
- [5] Eli Megidish, Joseph Broz, Nicole Greene, and Hartmut Häffner, “Improved test of local lorentz invariance from a deterministic preparation of entangled states,” *Phys. Rev. Lett.* **122**, 123605 (2019).
- [6] Yi-Quan Zou, Ling-Na Wu, Qi Liu, Xin-Yu Luo, Shuai-Feng Guo, Jia-Hao Cao, Meng Khoon Tey, and Li You, “Beating the classical precision limit with spin-1 dicker states of more than 10,000 atoms,” *Proceedings of the National Academy of Sciences* **115**, 6381–6385 (2018).
- [7] Carlton M. Caves, “Quantum-mechanical noise in an interferometer,” *Phys. Rev. D* **23**, 1693–1708 (1981).
- [8] Nils J. Engelsens, Rajiv Krishnakumar, Onur Hosten, and Mark A. Kasevich, “Bell correlations in spin-squeezed states of 500 000 atoms,” *Phys. Rev. Lett.* **118**, 140401 (2017).
- [9] Samuel P. Nolan, Stuart S. Szigeti, and Simon A. Haine, “Optimal and robust quantum metrology using interaction-based readouts,” *Phys. Rev. Lett.* **119**, 193601 (2017).
- [10] Lin Jiao, Wei Wu, Si-Yuan Bai, and Jun-Hong An, “Quantum metrology in the noisy intermediate-scale quantum era,” *Advanced Quantum Technologies* **n/a**, 2300218.
- [11] S. F. Huelga, C. Macchiavello, T. Pellizzari, A. K. Ekert, M. B. Plenio, and J. I. Cirac, “Improvement of frequency standards with quantum entanglement,” *Phys. Rev. Lett.* **79**, 3865–3868 (1997).
- [12] Yuichiro Matsuzaki, Simon Benjamin, Shojun Nakayama, Shiro Saito, and William J. Munro, “Quantum metrology beyond the classical limit under the effect of dephasing,” *Phys. Rev. Lett.* **120**, 140501 (2018).
- [13] Alex W. Chin, Susana F. Huelga, and Martin B. Plenio, “Quantum metrology in non-markovian environments,” *Phys. Rev. Lett.* **109**, 233601 (2012).
- [14] Jia-Xin Peng, Baiqiang Zhu, Weiping Zhang, and Keyue Zhang, “Enhanced quantum metrology with non-phase-covariant noise,” *Phys. Rev. Lett.* **133**, 090801 (2024).
- [15] Matteo G A Paris, “Achieving the landau bound to precision of quantum thermometry in systems with vanishing gap,” *Journal of Physics A: Mathematical and Theoretical* **49**, 03LT02 (2015).
- [16] Luis A. Correa, Mohammad Mehboudi, Gerardo Adesso, and Anna Sanpera, “Individual quantum probes for optimal thermometry,” *Phys. Rev. Lett.* **114**, 220405 (2015).
- [17] Marlon Brenes and Dvira Segal, “Multispin probes for thermometry in the strong-coupling regime,” *Phys. Rev. A* **108**, 032220 (2023).
- [18] Patrick P. Potts, Jonathan Bohr Brask, and Nicolas Brunner, “Fundamental limits on low-temperature quantum thermometry with finite resolution,” *Quantum* **3**, 161 (2019).
- [19] Luis Pedro García-Pintos, Kishor Bharti, Jacob Bringe-watt, Hossein Dehghani, Adam Ehrenberg, Nicole Yunger Halpern, and Alexey V. Gorshkov, “Estimation of hamiltonian parameters from thermal states,” *Phys. Rev. Lett.* **133**, 040802 (2024).
- [20] J F Haase, A Smirne, J Kołodźński, R Demkowicz-Dobrzański, and S F Huelga, “Fundamental limits to frequency estimation: a comprehensive microscopic perspective,” *New Journal of Physics* **20**, 053009 (2018).
- [21] Wei Wu, Si-Yuan Bai, and Jun-Hong An, “Non-markovian sensing of a quantum reservoir,” *Phys. Rev. A* **103**, L010601 (2021).
- [22] Wei Wu, Zhen Peng, Si-Yuan Bai, and Jun-Hong An, “Threshold for a discrete-variable sensor of quantum reservoirs,” *Phys. Rev. Appl.* **15**, 054042 (2021).
- [23] Dario Tamascelli, Claudia Benedetti, Heinz-Peter Breuer, and Matteo G A Paris, “Quantum probing beyond pure dephasing,” *New Journal of Physics* **22**, 083027 (2020).
- [24] Marcin Jarzyna and Marcin Zwierz, “Parameter estimation in the presence of the most general gaussian dissipative reservoir,” *Phys. Rev. A* **95**, 012109 (2017).
- [25] Matteo Bina, Federico Grasselli, and Matteo G. A. Paris, “Continuous-variable quantum probes for structured environments,” *Phys. Rev. A* **97**, 012125 (2018).
- [26] Claudia Benedetti, Fahimeh Salari Sehbaran, Mohammad H. Zandi, and Matteo G. A. Paris, “Quantum probes for the cutoff frequency of ohmic environments,” *Phys. Rev. A* **97**, 012126 (2018).
- [27] Mamiko Tatsuta, Yuichiro Matsuzaki, and Akira Shimizu, “Quantum metrology with generalized cat states,” *Phys. Rev. A* **100**, 032318 (2019).
- [28] Yoshitaka Tanimura, “Numerically “exact” approach to open quantum dynamics: The hierarchical equations of motion (HEOM),” *The Journal of Chemical Physics* **153**, 020901 (2020).
- [29] Yang Zhao, “The hierarchy of Davydov’s Ansätze: From guesswork to numerically “exact” many-body wave functions,” *The Journal of Chemical Physics* **158**, 080901 (2023).
- [30] Kirill A. Velizhanin, Haobin Wang, and Michael Thoss, “Heat transport through model molecular junctions: A multilayer multiconfiguration time-dependent hartree ap-

- proach,” *Chemical Physics Letters* **460**, 325–330 (2008).
- [31] Arend G. Dijkstra and Yoshitaka Tanimura, “Non-markovian entanglement dynamics in the presence of system-bath coherence,” *Phys. Rev. Lett.* **104**, 250401 (2010).
- [32] Arend G. Dijkstra and Yoshitaka Tanimura, “System bath correlations and the nonlinear response of qubits,” *Journal of the Physical Society of Japan* **81**, 063301 (2012).
- [33] Jake Iles-Smith, Neill Lambert, and Ahsan Nazir, “Environmental dynamics, correlations, and the emergence of noncanonical equilibrium states in open quantum systems,” *Phys. Rev. A* **90**, 032114 (2014).
- [34] Luis A. Correa, Martí Perarnau-Llobet, Karen V. Hovhannisyanyan, Senaida Hernández-Santana, Mohammad Mehboudi, and Anna Sanpera, “Enhancement of low-temperature thermometry by strong coupling,” *Phys. Rev. A* **96**, 062103 (2017).
- [35] Qing-Shou Tan, Xulin Liu, Lan Xu, Wei Wu, and Le-Man Kuang, “Enhancement of sensitivity in low-temperature quantum thermometry via reinforcement learning,” *Phys. Rev. A* **109**, 042417 (2024).
- [36] Mathias R. Jørgensen, Patrick P. Potts, Matteo G. A. Paris, and Jonatan B. Brask, “Tight bound on finite-resolution quantum thermometry at low temperatures,” *Phys. Rev. Res.* **2**, 033394 (2020).
- [37] Guim Planella, Marina F. B. Cenni, Antonio Acín, and Mohammad Mehboudi, “Bath-induced correlations enhance thermometry precision at low temperatures,” *Phys. Rev. Lett.* **128**, 040502 (2022).
- [38] Marco Gabbriellini, Augusto Smerzi, and Luca Pezzè, “Multipartite entanglement at finite temperature,” *Scientific Reports* **8**, 15663 (2018).
- [39] Giulio Salvatori, Antonio Mandarino, and Matteo G. A. Paris, “Quantum metrology in lipkin-meshkov-glick critical systems,” *Phys. Rev. A* **90**, 022111 (2014).
- [40] Y.P. Ren, Z.J. Zhao, X. Yang, G.H. Wang, Y.D. Leng, G.J. Gao, and X.M. Liu, “Quantum fisher information at finite temperatures and the critical properties in ising-heisenberg diamond chain,” *Results in Physics* **37**, 105542 (2022).
- [41] Mohammad Mehboudi, Luis A. Correa, and Anna Sanpera, “Achieving sub-shot-noise sensing at finite temperatures,” *Phys. Rev. A* **94**, 042121 (2016).
- [42] Xian-Ting Liang, “Decoherence and relaxation of a qubit coupled to an ohmic bath directly and via an intermediate harmonic oscillator,” *Chemical Physics Letters* **449**, 296–303 (2007).
- [43] Jake Iles-Smith, Arend G. Dijkstra, Neill Lambert, and Ahsan Nazir, “Energy transfer in structured and unstructured environments: Master equations beyond the Born-Markov approximations,” *The Journal of Chemical Physics* **144**, 044110 (2016).
- [44] R. Martinazzo, B. Vacchini, K. H. Hughes, and I. Burghardt, “Communication: Universal Markovian reduction of Brownian particle dynamics,” *The Journal of Chemical Physics* **134**, 011101 (2011).
- [45] Nicholas Anto-Sztrikacs and Dvira Segal, “Capturing non-markovian dynamics with the reaction coordinate method,” *Phys. Rev. A* **104**, 052617 (2021).
- [46] Philipp Strasberg, Gernot Schaller, Neill Lambert, and Tobias Brandes, “Nonequilibrium thermodynamics in the strong coupling and non-markovian regime based on a reaction coordinate mapping,” *New Journal of Physics* **18**, 073007 (2016).
- [47] Yi-Da Sha and Wei Wu, “Continuous-variable quantum sensing of a dissipative reservoir,” *Phys. Rev. Res.* **4**, 023169 (2022).
- [48] Chun-Jie Yang, Jun-Hong An, Hong-Gang Luo, Yading Li, and C. H. Oh, “Canonical versus noncanonical equilibration dynamics of open quantum systems,” *Phys. Rev. E* **90**, 022122 (2014).
- [49] Yuan-Sheng Wang, Chong Chen, and Jun-Hong An, “Quantum metrology in local dissipative environments,” *New Journal of Physics* **19**, 113019 (2017).
- [50] H. Hainzer, D. Kiesenhofer, T. Ollikainen, M. Bock, F. Kranzl, M. K. Joshi, G. Yoeli, R. Blatt, T. Gefen, and C. F. Roos, “Correlation spectroscopy with multiqubit-enhanced phase estimation,” *Phys. Rev. X* **14**, 011033 (2024).
- [51] H. P. Breuer and F. Petruccione, *The Theory of Open Quantum Systems* (Oxford University Press, Oxford, 2002).
- [52] J. D. Cresser and J. Anders, “Weak and ultrastrong coupling limits of the quantum mean force gibbs state,” *Phys. Rev. Lett.* **127**, 250601 (2021).
- [53] Chee Kong Lee, Jeremy Moix, and Jianshu Cao, “Accuracy of second order perturbation theory in the polaron and variational polaron frames,” *The Journal of Chemical Physics* **136**, 204120 (2012).
- [54] Wei Wu and Chuan Shi, “Quantum parameter estimation in a dissipative environment,” *Phys. Rev. A* **102**, 032607 (2020).
- [55] K. Berrada, “Non-markovian effect on the precision of parameter estimation,” *Phys. Rev. A* **88**, 035806 (2013).
- [56] Marlon Brenes, Brett Min, Nicholas Anto-Sztrikacs, Nir Bar-Gill, and Dvira Segal, “Bath-induced interactions and transient dynamics in open quantum systems at strong coupling: Effective Hamiltonian approach,” *The Journal of Chemical Physics* **160**, 244106 (2024).
- [57] Nicholas Anto-Sztrikacs, Ahsan Nazir, and Dvira Segal, “Effective-hamiltonian theory of open quantum systems at strong coupling,” *PRX Quantum* **4**, 020307 (2023).
- [58] M. P. Woods, R. Groux, A. W. Chin, S. F. Huelga, and M. B. Plenio, “Mappings of open quantum systems onto chain representations and Markovian embeddings,” *Journal of Mathematical Physics* **55**, 032101 (2014).
- [59] See the Supplemental Materials for more details on the reaction-coordinate-mapping approach, the calculations of the SNR, the GRWA approach, the proof for the universality of the T^{-1} -scaling relation in the finite- N cases, as well as the thermodynamic properties of the Dicke model case.
- [60] E. K. Twyeffort Irish, “Generalized rotating-wave approximation for arbitrarily large coupling,” *Phys. Rev. Lett.* **99**, 173601 (2007).
- [61] Lixian Yu, Shiqun Zhu, Qifeng Liang, Gang Chen, and Suotang Jia, “Analytical solutions for the rabi model,” *Phys. Rev. A* **86**, 015803 (2012).
- [62] Yu-Yu Zhang and Qing-Hu Chen, “Generalized rotating-wave approximation for the two-qubit quantum rabi model,” *Phys. Rev. A* **91**, 013814 (2015).
- [63] Yu-Yu Zhang, Xiang-You Chen, Shu He, and Qing-Hu Chen, “Analytical solutions and genuine multipartite entanglement of the three-qubit dicke model,” *Phys. Rev. A* **94**, 012317 (2016).
- [64] I. I. Rabi, “On the process of space quantization,” *Phys. Rev.* **49**, 324–328 (1936).

- [65] I. I. Rabi, “Space quantization in a gyrating magnetic field,” *Phys. Rev.* **51**, 652–654 (1937).
- [66] Qiongtao Xie, Honghua Zhong, Murray T Batchelor, and Chaohong Lee, “The quantum rabi model: solution and dynamics,” *Journal of Physics A: Mathematical and Theoretical* **50**, 113001 (2017).
- [67] Fumiki Yoshihara, Tomoko Fuse, Sahel Ashhab, Kosuke Kakuyanagi, Shiro Saito, and Kouichi Semba, “Superconducting qubit–oscillator circuit beyond the ultrastrong-coupling regime,” *Nature Physics* **13**, 44–47 (2017).
- [68] Ning Zhang, Chong Chen, Si-Yuan Bai, Wei Wu, and Jun-Hong An, “Non-markovian quantum thermometry,” *Phys. Rev. Appl.* **17**, 034073 (2022).
- [69] R. H. Dicke, “Coherence in spontaneous radiation processes,” *Phys. Rev.* **93**, 99–110 (1954).
- [70] Y. K. Wang and F. T. Hioe, “Phase transition in the dicke model of superradiance,” *Phys. Rev. A* **7**, 831–836 (1973).
- [71] G. Comer Duncan, “Effect of antiresonant atom-field interactions on phase transitions in the dicke model,” *Phys. Rev. A* **9**, 418–421 (1974).
- [72] Giuseppe Liberti and Rosa Letizia Zaffino, “Critical properties of two-level atom systems interacting with a radiation field,” *Phys. Rev. A* **70**, 033808 (2004).
- [73] G. Liberti and R. L. Zaffino, “Thermodynamic properties of the dicke model in the strong-coupling regime,” *The European Physical Journal B - Condensed Matter and Complex Systems* **44**, 535–541 (2005).
- [74] Jian Ma and Xiaoguang Wang, “Fisher information and spin squeezing in the lipkin-meshkov-glick model,” *Phys. Rev. A* **80**, 012318 (2009).
- [75] Carmen Invernizzi, Michael Korbman, Lorenzo Campos Venuti, and Matteo G. A. Paris, “Optimal quantum estimation in spin systems at criticality,” *Phys. Rev. A* **78**, 042106 (2008).
- [76] Paolo Zanardi, Matteo G. A. Paris, and Lorenzo Campos Venuti, “Quantum criticality as a resource for quantum estimation,” *Phys. Rev. A* **78**, 042105 (2008).
- [77] Teng-Long Wang, Ling-Na Wu, Wen Yang, Guang-Ri Jin, Neill Lambert, and Franco Nori, “Quantum fisher information as a signature of the superradiant quantum phase transition,” *New Journal of Physics* **16**, 063039 (2014).
- [78] M. Bina, I. Amelio, and M. G. A. Paris, “Dicke coupling by feasible local measurements at the superradiant quantum phase transition,” *Phys. Rev. E* **93**, 052118 (2016).
- [79] Marek M. Rams, Piotr Sierant, Omyoti Dutta, Paweł Horodecki, and Jakub Zakrzewski, “At the limits of criticality-based quantum metrology: Apparent superheisenberg scaling revisited,” *Phys. Rev. X* **8**, 021022 (2018).
- [80] Irénée Frérot and Tommaso Roscilde, “Quantum critical metrology,” *Phys. Rev. Lett.* **121**, 020402 (2018).
- [81] Ahsan Nazir and Gernot Schaller, “The reaction coordinate mapping in quantum thermodynamics,” in *Thermodynamics in the Quantum Regime: Fundamental Aspects and New Directions*, edited by Felix Binder, Luis A. Correa, Christian Gogolin, Janet Anders, and Gerardo Adesso (Springer International Publishing, Cham, 2018) pp. 551–577.
- [82] A. J. Leggett, “Quantum tunneling in the presence of an arbitrary linear dissipation mechanism,” *Phys. Rev. B* **30**, 1208–1218 (1984).
- [83] F Cerisola, M Berritta, S Scali, S A R Horsley, J D Cresser, and J Anders, “Quantum–classical correspondence in spin–boson equilibrium states at arbitrary coupling,” *New Journal of Physics* **26**, 053032 (2024).
- [84] Marcin Lobejko, Marek Winczewski, Gerardo Suárez, Robert Alicki, and Michał Horodecki, “Corrections to the hamiltonian induced by finite-strength coupling to the environment,” *Phys. Rev. E* **110**, 014144 (2024).
- [85] Maoxin Liu, Zu-Jian Ying, Jun-Hong An, and Hong-Gang Luo, “Mean photon number dependent variational method to the rabi model,” *New Journal of Physics* **17**, 043001 (2015).
- [86] Bin-Bin Mao, Liangsheng Li, Yimin Wang, Wen-Long You, Wei Wu, Maoxin Liu, and Hong-Gang Luo, “Variational generalized rotating-wave approximation in the two-qubit quantum rabi model,” *Phys. Rev. A* **99**, 033834 (2019).
- [87] Ze-Zhou Zhang and Wei Wu, “Work statistics and thermal phase transitions,” *Phys. Rev. E* **106**, 034104 (2022).
- [88] T. Holstein and H. Primakoff, “Field dependence of the intrinsic domain magnetization of a ferromagnet,” *Phys. Rev.* **58**, 1098–1113 (1940).
- [89] Clive Emary and Tobias Brandes, “Chaos and the quantum phase transition in the dicke model,” *Phys. Rev. E* **67**, 066203 (2003).

Supplemental Materials for “Low-temperature Quantum Metrology Enhanced by Strong Couplings”

This Supplemental Materials provides more details on the reaction-coordinate-mapping approach, the calculations of the SNR, the GRWA approach, the proof for the universality of the T^{-1} -scaling relation in the finite-N cases, as well as the thermodynamic properties of the Dicke model case.

The reaction-coordinate-mapping approach

The reaction-coordinate mapping can be viewed as a unitary transformation, which maps the original Hamiltonian

$$\hat{H} = \hat{H}_s + \sum_k \omega_k \hat{b}_k^\dagger \hat{b}_k + \hat{S} \sum_k g_k (\hat{b}_k^\dagger + \hat{b}_k) \quad (12)$$

into a new (mapped) Hamiltonian

$$\hat{\mathcal{H}} = \hat{H}_s + \omega \hat{a}^\dagger \hat{a} + g \hat{S} (\hat{a}^\dagger + \hat{a}) + \sum_k \tilde{\omega}_k \hat{a}^\dagger \hat{a}_k + (\hat{a}^\dagger + \hat{a}) \sum_k \tilde{g}_k (\hat{a}_k^\dagger + \hat{a}_k) + (\hat{a}^\dagger + \hat{a})^2 \sum_k \frac{\tilde{g}_k^2}{\tilde{\omega}_k}. \quad (13)$$

In the main text, $H_s = \epsilon \hat{J}_z$ and $\hat{S} = \hat{J}_x$, but we want to emphasize that the reaction-coordinate-mapping approach is universal to different forms of H_s and \hat{S} .

The relation between the spectral density of the original Hamiltonian $J(\varpi) = J^{(0)}(\varpi) = \sum_k g_k^2 \delta(\varpi - \omega_k)$ and the spectral density for the residual bath in $\hat{\mathcal{H}}$, which is defined by $\mathcal{J}(\varpi) = J^{(1)}(\varpi) = \sum_k \tilde{g}_k^2 \delta(\varpi - \tilde{\omega}_k)$, can be established via the dynamical equivalence between \hat{H} and $\hat{\mathcal{H}}$ [33, 81]. To see this, we first consider the Heisenberg equation of motion for an arbitrary system's operator \hat{Q} and the annihilate operators of the bath, namely \hat{b}_k , from the original Hamiltonian \hat{H} as follows

$$\dot{\hat{Q}} = i[\hat{H}, \hat{Q}] = i\hat{Q}_1 + i\hat{Q}_0 \sum_k g_k (\hat{b}_k^\dagger + \hat{b}_k), \quad (14)$$

$$i\dot{\hat{b}}_k = i[\hat{H}, \hat{b}_k] = -i\omega_k \hat{b}_k - ig_k \hat{S}, \quad (15)$$

where $\hat{Q}_0 = [\hat{S}, \hat{Q}]$ and $\hat{Q}_1 = [\hat{H}_s, \hat{Q}]$. Applying the Laplace-Fourier transformation, which is introduced as $f(z) = \int_0^\infty f(t) e^{izt} dt$, to the above two equations, one sees

$$iz\hat{Q}(z) = i\hat{Q}_1(z) + \frac{i}{2\pi} \int_0^\infty \hat{Q}_0(z') \sum_k g_k [\hat{b}_k^\dagger(z-z') + \hat{b}_k(z-z')] dz', \quad (16)$$

$$iz\hat{b}_k(z) = -i\omega_k \hat{b}_k(z) - ig_k \hat{S}(z), \quad (17)$$

By solving the last equation with $\hat{b}_k(z) = -\frac{g_k}{z+\omega_k} \hat{S}(z)$, and inserting it into the first equation, one finds

$$\begin{aligned} z\hat{Q}(z) &= \hat{Q}_1(z) + \frac{1}{2\pi} \int_0^\infty \hat{Q}_0(z') \sum_k \left[\frac{g_k^2}{z-z'-\omega_k} - \frac{g_k^2}{z-z'+\omega_k} \right] \hat{S}(z-z') dz', \\ &= \hat{Q}_1(z) + \frac{1}{2\pi} \int_0^\infty \hat{Q}_0(z') \left[\frac{1}{\pi} \int_0^\infty J^{(0)}(\varpi) \frac{\varpi}{(z-z')^2 - \varpi^2} d\varpi \right] \hat{S}(z-z') dz', \\ &= \hat{Q}_1(z) - \frac{1}{2\pi} \int_0^\infty \hat{Q}_0(z') \frac{1}{2} W^{(0)}(z-z') \hat{S}(z-z') dz'. \end{aligned} \quad (18)$$

Here, we have introduced the Cauchy transformation

$$W^{(n)}(z) = \frac{2}{\pi} \int_0^\infty J^{(n)}(\varpi) \frac{\varpi}{\varpi^2 - z^2} d\varpi = \frac{1}{\pi} \int_{-\infty}^\infty \frac{J^{(n)}(\varpi)}{\varpi - z} d\varpi, \quad (19)$$

where we have extended the integral boundary via the analytic continuation by introducing $J^{(n)}(\varpi) = -J^{(n)}(-\varpi)$ for $\varpi < 0$. Using the residue theorem, the spectral density $J^{(n)}(\varpi)$ can be expressed in terms of $W^{(n)}(z)$ as [33, 81, 82]

$$J^{(n)}(\varpi) = \lim_{\delta \rightarrow 0^+} \text{Im}[W^{(n)}(\varpi + i\delta)]. \quad (20)$$

Using the same method, from the Heisenberg equation of motion for the mapped Hamiltonian $\hat{\mathcal{H}}$, one can find the equation of motion for an arbitrary system's operator $\hat{\mathcal{Q}}$ in the Laplace-Fourier space as [81]

$$z\hat{\mathcal{Q}}(z) = \hat{\mathcal{Q}}_1(z) + \frac{1}{2\pi} \int_0^\infty \hat{\mathcal{Q}}_0(z') \frac{2g^2\omega}{(z-z')^2 - \omega^2 + \omega W^{(1)}(z-z')} \hat{S}(z-z') dz'. \quad (21)$$

Comparing Eq. (18) and Eq. (21), one can conclude that \hat{H} and $\hat{\mathcal{H}}$ are dynamically equivalent if

$$-\frac{1}{2}W^{(0)}(z-z') = \frac{2g^2\omega}{(z-z')^2 - \omega^2 + \omega W^{(1)}(z-z')}. \quad (22)$$

By employing the above equation as well as Eq. (20), the relation between $J^{(0)}(\varpi)$ and $J^{(1)}(\varpi)$ can be built.

The spectral density

In our work, we assume the spectral density with respect to the mapped Hamiltonian $\hat{\mathcal{H}}$, which defined as $J^{(1)}(\varpi) = \sum_k \tilde{g}_k^2 \delta(\varpi - \tilde{\omega}_k)$, has an Ohmic form as

$$J^{(1)}(\varpi) = \gamma\varpi e^{-\varpi/\omega_c}, \quad (23)$$

where γ is effective coupling strength and ω_c is cutoff frequency. With the help of the Eq. (22), we find $J^{(0)}(\varpi)$ has a standard Lorentzian form as follows

$$\begin{aligned} J^{(0)}(\varpi) &= \lim_{\delta \rightarrow 0^+} \text{Im} \frac{-4g^2\omega}{(\varpi + i\delta)^2 - \omega^2 + \omega W^{(1)}(\varpi + i\delta)} \\ &= \frac{4\gamma\omega^2 g^2 \varpi}{(\varpi^2 - \omega^2)^2 + (\gamma\omega\varpi)^2} = \frac{\Gamma\zeta\varpi}{(\varpi^2 - \omega^2)^2 + \Gamma^2\varpi^2}, \end{aligned} \quad (24)$$

where ω is the resonant frequency, $\Gamma = \gamma\omega$ is the peak width and $\zeta = 4\omega g^2$ can be viewed as the effective probe-bath coupling strength.

By appropriately choosing the parameters of $\{\zeta, \Gamma, \omega\}$, one can realize an arbitrarily strong probe-bath coupling in the original Hamiltonian \hat{H} with an arbitrarily large ζ , while having arbitrarily small coupling between $\hat{\mathcal{H}}_s$ and $\hat{\mathcal{H}}_b$ with an arbitrarily small γ . The above operation can be done because the condition of $\gamma \rightarrow 0$ is achievable via choosing $\Gamma/\omega \rightarrow 0$, which does not imply any constraint on the coupling strength ζ [83]. Thus, in the limit $\gamma \rightarrow 0$, while allowing ζ to be arbitrarily large, one can regard the extended composite system (the probe plus the RC mode) experiences a canonical thermalization, which results in $\varrho_s(\infty) = e^{-\beta\hat{\mathcal{H}}_s}/\mathcal{Z}$. Thus, the reaction-coordinate mapping recasts the non-Markovian dynamics of the probe into the Markovian dynamics of an enlarged system including the probe and an effective mode of the environment.

In the especial limit $g \rightarrow 0$, which means $\zeta \rightarrow 0$, one shall recover the usual weak-coupling result, i.e.,

$$\lim_{g \rightarrow 0} \text{Tr}_{\text{RC}}[\varrho_s(\infty)] = \rho_s^{\text{weak}}(\infty) = \frac{e^{-\beta\hat{\mathcal{H}}_s}}{\mathcal{Z}}. \quad (25)$$

To check the above conclusion, in Fig. 4, we plot the average value of \hat{J}_z from the weak-coupling approximation, i.e., $\langle \hat{J}_z \rangle_{\text{weak}} = \text{Tr}[\rho_s^{\text{weak}}(\infty)\hat{J}_z]$ and the reaction coordinate mapping approach, i.e., $\langle \hat{J}_z \rangle = \text{Tr}[\varrho_s(\infty)\hat{J}_z]$, versus the bath temperature. Good agreement is found between results from $\langle \hat{J}_z \rangle_{\text{weak}}$ and $\langle \hat{J}_z \rangle$ when g is small. However, as the g becomes large, a distinct deviation can be observed, which means the noncanonical effect induced by the strong couplings becomes non-negligible.

The SNR

By using the reaction-coordinate mapping, the long-time steady state of the probe in the strong-coupling regime is corrected as the reduced Gibbs state with respect to the Hamiltonian of the extended composite system, consisting of the probe and the RC mode, as [17, 33, 43, 56, 84]

$$\rho_s(\infty) = \text{Tr}_{\text{RC}} \left(\frac{e^{-\beta\hat{\mathcal{H}}_s}}{\mathcal{Z}} \right), \quad (26)$$

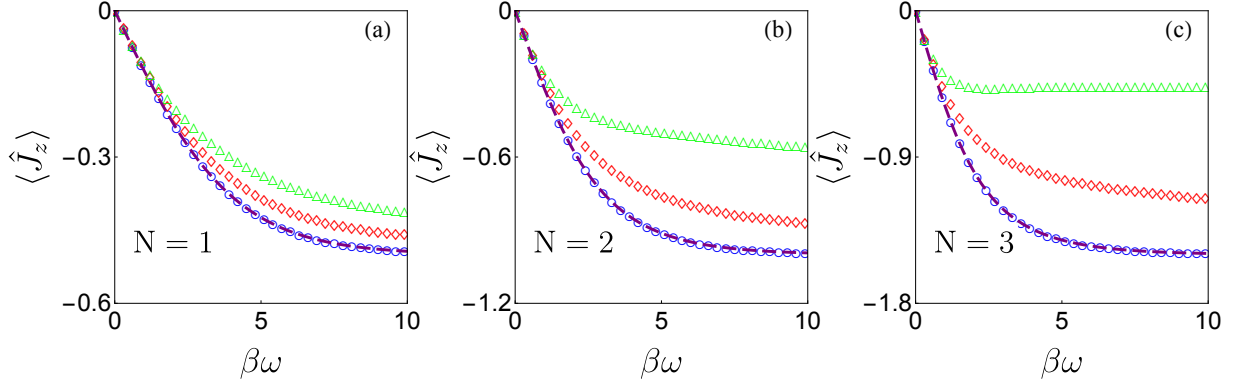


FIG. 4. The average values of $\langle \hat{J}_z \rangle$ are plotted as a function of the bath temperature $\beta\omega$ with $\epsilon = 0.5\Delta$ for different spin numbers: (a) $N = 1$, (b) $N = 2$ and (c) $N = 3$. The purple dashed lines are results from the weak-coupling treatment, while the blue circles ($g = 0.01\omega$), the red diamonds ($g = 0.5\omega$) and the green triangles ($g = 0.8\omega$) are exact numerical results from the reaction coordinate mapping approach.

where \mathcal{Z} denotes the partition function $\mathcal{Z} = \text{Tr}(e^{-\beta\hat{\mathcal{H}}_s})$. Then, the expression of $\langle \hat{J}_z \rangle$ can be derived as

$$\langle \hat{J}_z \rangle = \text{Tr}_s[\rho_s(\infty)\hat{J}_z] = \frac{1}{\mathcal{Z}} \text{Tr}(e^{-\beta\hat{\mathcal{H}}_s} \hat{J}_z) = -\frac{1}{\beta} \frac{\partial}{\partial \epsilon} \ln \mathcal{Z}. \quad (27)$$

Similarly, one sees

$$\langle \hat{J}_z^2 \rangle = \frac{1}{\mathcal{Z}\beta^2} \frac{\partial^2 \mathcal{Z}}{\partial \epsilon^2}. \quad (28)$$

Thus, as long as the partition function is obtained, the corresponding SNR can be accordingly derived. Technically speaking, the partition function can be obtained by numerically diagonalizing $\hat{\mathcal{H}}_s$. However, such a purely numerical treatment may miss some important physics. To build a more clear picture, in this section, we provide an analytical way to compute the partition function using the generalized rotating-wave approximation (GRWA) approach [60, 62, 63].

The Generalized Rotating-Wave Approximation

When the probe-RC mode coupling is not too strong, the character of the energy spectrum of $\hat{\mathcal{H}}_s$ can be accurately described by the GRWA approach (see the comparisons between the GRWA result and the exact result by numerically diagonalizing $\hat{\mathcal{H}}_s$ in Fig. 5.), which provides an analytical result maintaining strong links to the familiar language and techniques of quantum optics [60]. To perform the GRWA approach, we first apply an unitary transformation to the Hamiltonian of $\hat{\mathcal{H}}_s$ as

$$\hat{\mathcal{H}}'_s = e^{\lambda\hat{J}_x(\hat{a}^\dagger - \hat{a})} \hat{\mathcal{H}}_s e^{-\lambda\hat{J}_x(\hat{a}^\dagger - \hat{a})}, \quad (29)$$

where λ is a variational parameter and will be determined later. The transformed Hamiltonian $\hat{\mathcal{H}}'_s$ is given by

$$\hat{\mathcal{H}}'_s = \omega\hat{a}^\dagger\hat{a} + (\omega\lambda^2 - 2\lambda g)\hat{J}_x^2 + (g - \omega\lambda)\hat{J}_x(\hat{a}^\dagger + \hat{a}) + \epsilon\{\hat{J}_z \cosh[\lambda(\hat{a}^\dagger - \hat{a})] - i\hat{J}_y \sinh[\lambda(\hat{a}^\dagger - \hat{a})]\}. \quad (30)$$

Following Refs. [85, 86], we expand the hyperbolic cosine and sine terms as follows

$$\cosh[\lambda(\hat{a}^\dagger - \hat{a})] = F_0(\hat{a}^\dagger\hat{a}) + \sum_{n=1}^{\infty} [(a^\dagger)^{2n} F_{2n}(\hat{a}^\dagger\hat{a}) - F_{2n}(\hat{a}^\dagger\hat{a})\hat{a}^{2n}], \quad (31)$$

$$\sinh[\lambda(\hat{a}^\dagger - \hat{a})] = \sum_{n=0}^{\infty} [(a^\dagger)^{2n+1} F_{2n+1}(\hat{a}^\dagger\hat{a}) - F_{2n+1}(\hat{a}^\dagger\hat{a})\hat{a}^{2n+1}], \quad (32)$$

where the function $F_n(m)$ is defined by

$$F_n(m) \equiv \lambda^n e^{-\frac{1}{2}\lambda^2} \frac{m!}{(m+n)!} L_m^n(\lambda^2) \quad (33)$$

with $L_m^n(x)$ being the associated Laguerre polynomials

$$L_m^n(x) \equiv \sum_{j=0}^m \frac{(n+m)!}{(n+j)!(m-j)!j!} (-x)^j. \quad (34)$$

Using these expanded expressions, one can drop all the higher-order terms of $(\hat{a}^\dagger)^l \hat{a}^{l'}$ with $l, l' \geq 2$, which results in $\hat{\mathcal{H}}'_s \simeq \hat{\mathcal{H}}'_0 + \hat{\mathcal{H}}'_{\text{RWA}} + \hat{\mathcal{H}}'_{\text{CRW}}$, where

$$\hat{\mathcal{H}}'_0 = \omega \hat{a}^\dagger \hat{a} + (\omega \lambda^2 - 2\lambda g) \hat{J}_x^2 + \epsilon \hat{J}_z F_0(\hat{a}^\dagger \hat{a}), \quad (35)$$

is the zero-order (also called the adiabatic) term, and

$$\hat{\mathcal{H}}'_{\text{RWA}} = \frac{1}{2}(g - \omega \lambda)(\hat{J}_- \hat{a}^\dagger + \hat{J}_+ \hat{a}) + \frac{1}{2}\epsilon \left[\hat{J}_- \hat{a}^\dagger F_1(\hat{a}^\dagger \hat{a}) + \hat{J}_+ F_1(\hat{a}^\dagger \hat{a}) \hat{a} \right], \quad (36)$$

is the generalized rotating-wave-approximation term with $\hat{J}_\pm \equiv \frac{1}{2}(\hat{J}_z \pm i\hat{J}_y)$, which conserves the total excitation and

$$\hat{\mathcal{H}}'_{\text{CRW}} = \frac{1}{2}(g - \omega \lambda)(\hat{J}_- \hat{a} + \hat{J}_+ \hat{a}^\dagger) - \frac{1}{2}\epsilon \left[\hat{J}_- F_1(\hat{a}^\dagger \hat{a}) \hat{a} + \hat{J}_+ \hat{a}^\dagger F_1(\hat{a}^\dagger \hat{a}) \right], \quad (37)$$

is the term containing the generalized counter-rotating-wave terms. In the GRWA treatment, one neglects the contribution from $\hat{\mathcal{H}}'_{\text{CRW}}$ and finally obtain the effective GRWA Hamiltonian as $\hat{\mathcal{H}}_{\text{GRWA}} = \hat{\mathcal{H}}'_0 + \hat{\mathcal{H}}'_{\text{RWA}}$, which finally recovers Eq. (6) in the main text.

Taking the direct product basis $|m, n\rangle \equiv |m\rangle \otimes |n\rangle$ with $\hat{J}_z |m\rangle = m|m\rangle$ and $\hat{a}^\dagger \hat{a} |n\rangle = n|n\rangle$, the approximate ground state of composite system $\hat{\mathcal{H}}_s$ within the treatment of the GRWA approach is then given by

$$|E_g\rangle \simeq |E_g^{\text{GRWA}}\rangle = e^{-\lambda \hat{J}_x (\hat{a}^\dagger - \hat{a})} \left| -\frac{N}{2}, 0 \right\rangle, \quad (38)$$

and the corresponding ground-state energy reads

$$\begin{aligned} E_g \simeq E_g^{\text{GRWA}} &= \left\langle -\frac{N}{2}, 0 \left| \hat{\mathcal{H}}'_0 + \hat{\mathcal{H}}'_{\text{RWA}} \right| -\frac{N}{2}, 0 \right\rangle \\ &= \frac{N}{4}(\omega \lambda^2 - 2g\lambda) - \frac{N}{2}\epsilon e^{-\frac{1}{2}\lambda^2}. \end{aligned} \quad (39)$$

The other way to compute the ground-state energy is straightforwardly diagonalize $\hat{\mathcal{H}}'_0$ in the product basis $\{|m, n\rangle\}$. These two methods yields the same physical results.

Up to here, the only task left to be completed is determining the variational parameter λ . Following Refs. [85, 86], the parameter λ is determined by minimizing the ground-state energy E_g^{GRWA} as $\partial_\lambda E_g^{\text{GRWA}} = 0$, which yields

$$\lambda - \frac{g}{\omega} - \frac{\epsilon \lambda}{\omega} e^{-\frac{1}{2}\lambda^2} = 0. \quad (40)$$

By numerically solving the above transcendental equation, the value of λ is then determined, which fully completes the GRWA approach. Moreover, Eq. (40) has an approximate solution as [85, 86]

$$\lambda = \frac{g}{\omega + \epsilon e^{-\frac{1}{2}\lambda_0}}, \quad (41)$$

where $\lambda_0 \equiv g/(\epsilon + \omega)$. This approximate solution can be used as a benchmark to testify the validity of purely numerical simulations. As plotted in Fig. 6 (a), a good agreement is found between the approximate solution predicted by Eq. (40) and the purely numerical simulation from solving Eq. (41).

Next, we apply the GRWA approach to the cases of $N = 1, 2, 3$ and display the analytical expressions of the partition function in the three cases, from which the SNRs can be accordingly derived.

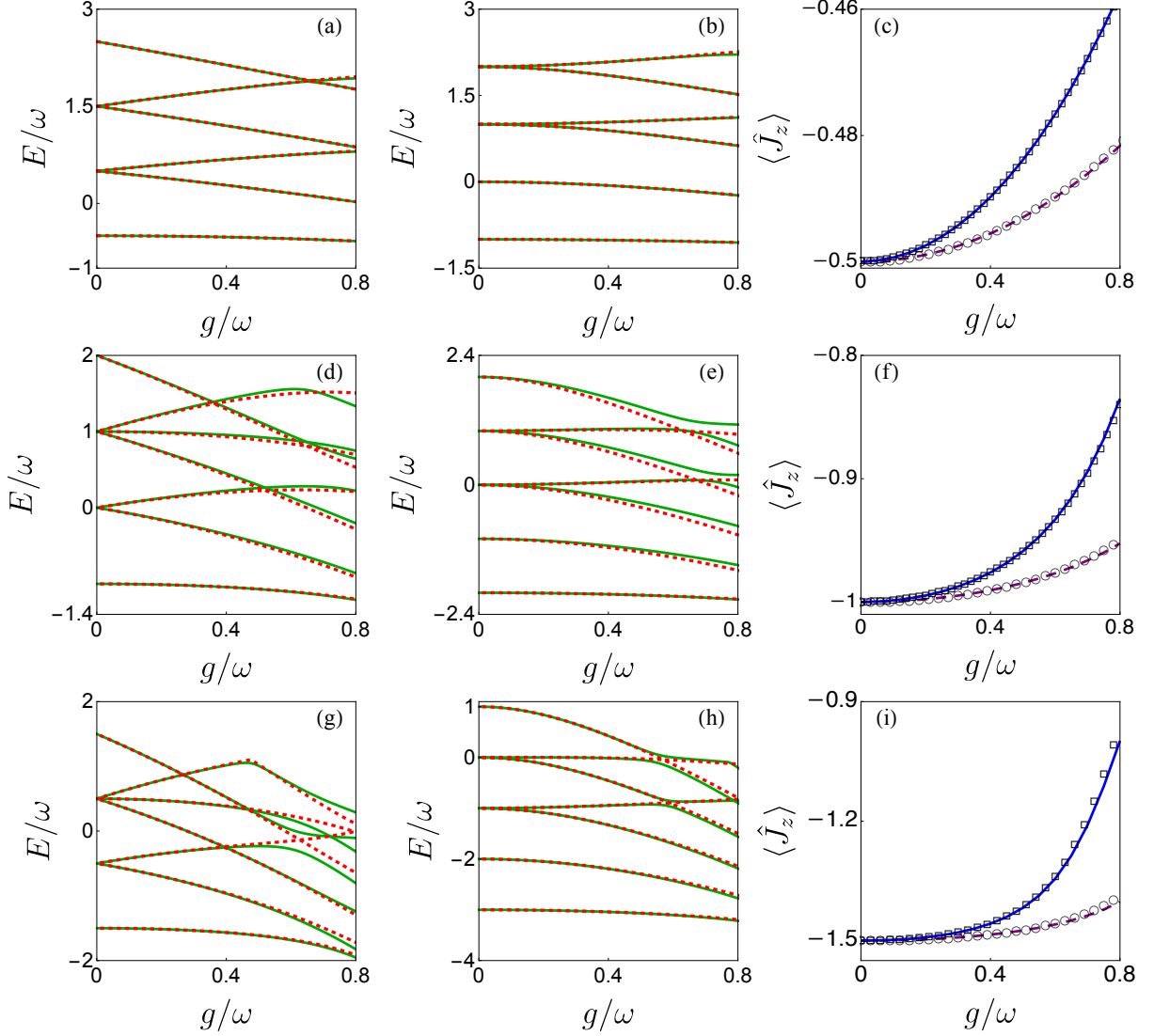


FIG. 5. Energy levels obtained by the GRWA approach (red dashed lines) and the numerically exact diagonalization (green solid lines) are plotted for comparison for different ϵ/ω and $N = 1$: (a) $\epsilon/\omega = 1$ and $N = 1$, (b) $\epsilon/\omega = 2$ and $N = 1$, (d) $\epsilon/\omega = 1$ and $N = 2$, (e) $\epsilon/\omega = 2$ and $N = 2$, (g) $\epsilon/\omega = 1$ and $N = 3$ and (h) $\epsilon/\omega = 2$ and $N = 3$. The average value of the observable $\langle \hat{J}_z \rangle$ obtained by the numerically exact diagonalization is plotted as a function of g/ω with different ϵ/ω : $\epsilon/\omega = 1$ (blue solid lines) and $\epsilon/\omega = 2$ (purple dashed lines). The squares and the circles are analytical results predicted by the GRWA approach.

$N = 1$ case

For the simplest case $N = 1$, the Hamiltonian of $\hat{\mathcal{H}}_{\text{GRWA}}^{N=1}$ is a block-diagonal matrix in the basis of $\{|g, n+1\rangle, |e, n\rangle\}$ with $|g\rangle$ and $|e\rangle$ being the eigenstates of Pauli operator $\hat{\sigma}_z$ as

$$\hat{\mathcal{H}}_{\text{GRWA}}^{N=1} = E_{g,\text{GRWA}}^{N=1} \mathbf{1} \oplus \hat{\mathfrak{H}}_{n=0}^{N=1} \oplus \hat{\mathfrak{H}}_{n=1}^{N=1} \oplus \hat{\mathfrak{H}}_{n=2}^{N=1} \dots, \quad (42)$$

where $E_{g,\text{GRWA}}^{N=1} = \langle g, 0 | \hat{\mathcal{H}}_{\text{GRWA}}^{N=1} | g, 0 \rangle$ is the ground-state energy, $\mathbf{1}$ is a 1×1 identity matrix and with $\hat{\mathfrak{H}}_n^{N=1}$ being 2×2 matrices as

$$\hat{\mathfrak{H}}_n^{N=1} = \begin{pmatrix} \xi_n^{N=1} & R_n^{N=1} \\ R_n^{N=1} & \xi_{n+1,-}^{N=1} \end{pmatrix}, \quad (43)$$

where

$$\xi_{n,\pm}^{N=1} = \omega n + \frac{1}{4}(\omega\lambda^2 - 2g\lambda) \pm \frac{1}{2}\epsilon F_0(n), \quad R_n^{N=1} = \frac{1}{2}\sqrt{n+1} \left[g - \omega\lambda + \epsilon F_1(n) \right]. \quad (44)$$

By diagonalizing these 2×2 matrices $\hat{\mathfrak{H}}_n^{N=1}$ by hand, the corresponding eigenvalues are

$$E_{n,\pm}^{N=1} = \frac{1}{2} \left[\xi_n^+ + \xi_{n+1}^- \pm \sqrt{4R_n^2 + (\xi_n^+ - \xi_{n+1}^-)^2} \right]. \quad (45)$$

Then, the partition function within the GRWA approach $\mathcal{Z}_{\text{GRWA}}^{N=1} = \text{Tr}(e^{-\beta\hat{\mathcal{H}}_{\text{GRWA}}^{N=1}})$ can be written as the sum of all these eigenenergies

$$\mathcal{Z}_{\text{GRWA}}^{N=1} = e^{-\beta E_{g,\text{GRWA}}^{N=1}} + \sum_{n=0}^{\infty} \sum_{\nu=\pm} e^{-\beta E_{n,\nu}^{N=1}}. \quad (46)$$

In Fig. 5 (c), we display the results of $\langle \hat{J}_z \rangle$ calculated by the numerically exact diagonalization method and the GRWA approach. No distinctly difference is found, which convinces us that the GRWA method truly captures the essential physics of the quantum Rabi model.

$N = 2$ case

In the case of $N = 2$, the Hamiltonian of $\hat{\mathcal{H}}_{\text{GRWA}}^{N=2}$ is a block-diagonal matrix as

$$\hat{\mathcal{H}}_{\text{GRWA}}^{N=2} = E_{g,\text{GRWA}}^{N=2} \mathbf{1} \oplus \hat{\mathfrak{H}}_{n=0}^{N=2} \oplus \hat{\mathfrak{H}}_{n=1}^{N=2} \oplus \hat{\mathfrak{H}}_{n=2}^{N=2} \dots, \quad (47)$$

where $\hat{\mathfrak{H}}_{n \geq 1}^{N=2}$ are 3×3 matrices in the basis of $\{|-1, n+1\rangle, |0, n\rangle, |1, n-1\rangle\}$

$$\hat{\mathfrak{H}}_{n \geq 1}^{N=2} = \begin{pmatrix} \xi_{n+1,-}^{N=2} & R_{n,0}^{N=2} & 0 \\ R_{n,0}^{N=2} & \xi_{n,0}^{N=2} & R_{n,1}^{N=2} \\ 0 & R_{n,1}^{N=2} & \xi_{n-1,+}^{N=2} \end{pmatrix} \quad (48)$$

with

$$\xi_{n,\pm}^{N=2} = \omega n + \frac{1}{2}(\omega\lambda^2 - 2g\lambda) \pm F_0(n), \quad \xi_{n,0}^{N=2} = \omega n + \omega\lambda^2 - 2g\lambda, \quad (49)$$

$$R_{n,0}^{N=2} = \frac{\sqrt{2(n+1)}}{2} \left[g - \lambda\omega + \epsilon F_1(n) \right], \quad R_{n,1}^{N=2} = \frac{\sqrt{2n}}{2} \left[g - \lambda\omega + \epsilon F_1(n-1) \right]. \quad (50)$$

And $\hat{\mathfrak{H}}_{n=0}^{N=2}$ is a 2×2 matrix in the basis $\{|-1, 1\rangle, |0, 0\rangle\}$ as

$$\hat{\mathfrak{H}}_{n=0}^{N=2} = \begin{pmatrix} \xi_{0,0}^{N=2} & R_{0,0}^{N=2} \\ R_{0,0}^{N=2} & \xi_{0,-}^{N=2} \end{pmatrix}. \quad (51)$$

By diagonalizing these 2×2 and 3×3 matrices, the analytical expression of the partition function can be derived similar to the case of $N = 1$.

$N = 3$ case

For the $N = 3$ case, the Hamiltonian of $\hat{\mathcal{H}}_{\text{GRWA}}^{N=3}$ is a block-diagonal matrix as

$$\hat{\mathcal{H}}_{\text{GRWA}}^{N=3} = E_{g,\text{GRWA}}^{N=3} \mathbf{1} \oplus \hat{\mathfrak{H}}_{n=0}^{N=3} \oplus \hat{\mathfrak{H}}_{n=1}^{N=3} \oplus \hat{\mathfrak{H}}_{n=2}^{N=3} \oplus \hat{\mathfrak{H}}_{n=3}^{N=3} \dots, \quad (52)$$

where $\hat{\mathfrak{H}}_{n \geq 2}^{N=3}$ are 4×4 matrices in the basis of $\{|-\frac{3}{2}, n+2\rangle, |-\frac{1}{2}, n+1\rangle, |\frac{1}{2}, n\rangle, |\frac{3}{2}, n-1\rangle\}$

$$\hat{\mathfrak{H}}_{n \geq 2}^{N=3} = \begin{pmatrix} \xi_{n+2,-}^{N=3} & R_{n,0}^{N=3} & 0 & 0 \\ R_{n,0}^{N=3} & \xi_{n+1,-}^{N=3} & R_{n,1}^{N=3} & 0 \\ 0 & R_{n,1}^{N=2} & \xi_{n,+}^{N=3} & R_{n,2}^{N=3} \\ 0 & 0 & R_{n,2}^{N=3} & \xi_{n-1,+}^{N=3} \end{pmatrix}, \quad (53)$$

with

$$\xi_{n,\pm}^{N=3} = \omega n + \frac{3}{4}(\omega\lambda^2 - 2g\lambda) \pm \frac{3}{2}\epsilon F_0(n), \quad \zeta_{n,\pm}^{N=3} = \omega n + \frac{7}{4}(\omega\lambda^2 - 2g\lambda) \pm \frac{1}{2}\epsilon F_0(n), \quad (54)$$

$$R_{n,0}^{N=3} = \frac{\sqrt{3(n+2)}}{2} [g - \lambda\omega + \epsilon F_1(n+1)], \quad R_{n,1}^{N=3} = \sqrt{n+1} [g - \lambda\omega + \epsilon F_1(n)], \quad R_{n,2}^{N=3} = \frac{\sqrt{3n}}{2} [g - \lambda\omega + \epsilon F_1(n-1)]. \quad (55)$$

And $\hat{\mathfrak{H}}_{n=1}^{N=3}$ is a 3×3 matrix in the basis $\{|-\frac{3}{2}, 2\rangle, |-\frac{1}{2}, 1\rangle, |\frac{1}{2}, 0\rangle\}$ as

$$\hat{\mathfrak{H}}_{n=1}^{N=3} = \begin{pmatrix} \xi_{2,-}^{N=3} & R_{0,0}^{N=3} & 0 \\ R_{0,0}^{N=3} & \zeta_{1,-}^{N=3} & R_{0,1}^{N=3} \\ 0 & R_{0,1}^{N=3} & \zeta_{0,+}^{N=3} \end{pmatrix}. \quad (56)$$

And $\hat{\mathfrak{H}}_{n=0}^{N=3}$ is a 2×2 matrix in the basis $\{|-\frac{3}{2}, 1\rangle, |-\frac{1}{2}, 0\rangle\}$ as

$$\hat{\mathfrak{H}}_{n=0}^{N=3} = \begin{pmatrix} \xi_{1,-}^{N=3} & R_{-1,0}^{N=3} \\ R_{-1,0}^{N=3} & \zeta_{0,-}^{N=3} \end{pmatrix}. \quad (57)$$

By diagonalizing these 2×2 , 3×3 and 4×4 matrices, the analytical expression of the partition function can be derived similar to the case of $N = 1$.

The Dicke model case

In this section, we shall discuss the thermodynamic properties of the Dicke model and derive the analytical expression of the SNR in the large- N limit. To this aim, we first introduce a renormalized coupling strength as $\bar{g} = \sqrt{N}g/2$ and reexpress the Hamiltonian of the Dicke model as

$$\begin{aligned} \hat{\mathcal{H}}_s &= \epsilon \hat{J}_z + \omega \hat{a}^\dagger \hat{a} + \frac{2\bar{g}}{\sqrt{N}} \hat{J}_x (\hat{a}^\dagger + \hat{a}) \\ &= \sum_{n=1}^N \left[\frac{\epsilon}{2} \hat{\sigma}_n^z + \omega \frac{\hat{a}^\dagger}{\sqrt{N}} \frac{\hat{a}}{\sqrt{N}} + \frac{\bar{g}}{\sqrt{N}} \hat{\sigma}_n^x (\hat{a} + \hat{a}^\dagger) \right]. \end{aligned} \quad (58)$$

Then, the partition function can be calculated as follows

$$\mathcal{Z}_{\text{DM}} = \text{Tr} \left(e^{-\beta \hat{\mathcal{H}}_s} \right) = \sum_{\sigma_1=g,e} \sum_{\sigma_2=g,e} \dots \sum_{\sigma_N=g,e} \langle \sigma_1 \sigma_2 \dots \sigma_N | \int_{-\infty}^{+\infty} \frac{d^2\alpha}{\pi} \langle \alpha | e^{-\beta \hat{\mathcal{H}}_s} | \alpha \rangle | \sigma_1 \sigma_2 \dots \sigma_N \rangle, \quad (59)$$

where $|\alpha\rangle$ introduced as the bosonic coherent state $\hat{a}|\alpha\rangle = \alpha|\alpha\rangle$. In the large- N limit, we have $\sqrt{N} \gg \max\{\epsilon, \omega, g\}$ which leads to

$$\begin{aligned} \langle \alpha | e^{-\beta \hat{\mathcal{H}}_s} | \alpha \rangle &\simeq \prod_n \left\langle \alpha \left| \exp \left\{ -\beta \left[\frac{\epsilon}{2} \hat{\sigma}_n^z + \omega \frac{\hat{a}^\dagger}{\sqrt{N}} \frac{\hat{a}}{\sqrt{N}} + \frac{\bar{g}}{\sqrt{N}} \hat{\sigma}_n^x (\hat{a} + \hat{a}^\dagger) \right] \right\} \right| \alpha \right\rangle \\ &\simeq \prod_n \exp \left\{ -\beta \left\langle \alpha \left| \left[\frac{\epsilon}{2} \hat{\sigma}_n^z + \omega \frac{\hat{a}^\dagger}{\sqrt{N}} \frac{\hat{a}}{\sqrt{N}} + \frac{\bar{g}}{\sqrt{N}} \hat{\sigma}_n^x (\hat{a} + \hat{a}^\dagger) \right] \right| \alpha \right\rangle \right\} \\ &= e^{-\beta\omega|\alpha|^2} \prod_n e^{-\beta \hat{O}_n}, \end{aligned} \quad (60)$$

where

$$\hat{O}_n = \frac{\epsilon}{2} \hat{\sigma}_n^z + \frac{2\bar{g}\text{Re}\alpha}{\sqrt{N}} \hat{\sigma}_n^x. \quad (61)$$

Thus, we have

$$\begin{aligned} \mathcal{Z}_{\text{DM}} &\simeq \int_{-\infty}^{+\infty} \frac{d^2\alpha}{\pi} e^{-\beta\omega|\alpha|^2} \left(\sum_{\sigma=\uparrow\downarrow} \langle \sigma | e^{-\beta \hat{O}_n} | \sigma \rangle \right)^N \\ &= \int_{-\infty}^{+\infty} \frac{d^2\alpha}{\pi} e^{-\beta\omega|\alpha|^2} \left\{ 2 \cosh \left[\beta \sqrt{\frac{\epsilon^2}{4} + \frac{4\bar{g}^2(\text{Re}\alpha)^2}{N}} \right] \right\}^N. \end{aligned} \quad (62)$$

To handle the complex integral, we introduce $x \equiv \text{Re}\alpha$ and $y \equiv \text{Im}\alpha$, which results in $d^2\alpha = dx dy$ and $|\alpha|^2 = x^2 + y^2$. By doing so, the y -part of the integral is a Gaussian integral and can be immediately carried out. Then, one finds

$$\mathcal{Z}_{\text{DM}} = \frac{1}{\sqrt{\pi\beta\omega}} \int_{-\infty}^{\infty} dx e^{-\beta\omega x^2} \left[2 \cosh \left(\beta \sqrt{\frac{\epsilon^2}{4} + \frac{4\bar{g}^2 x^2}{N}} \right) \right]^N. \quad (63)$$

The above expression is still intricate. We further use the steepest descent method or the so-called Laplace's integral method [72, 73, 87] to derive an approximate expression. To this aim, we replace x/\sqrt{N} by a new variable z , then the expression of \mathcal{Z}_{DM} can be rewritten as

$$\mathcal{Z}_{\text{DM}} = \sqrt{\frac{N}{\pi\beta\omega}} \int_{-\infty}^{\infty} dz e^{N\Phi(z)}, \quad (64)$$

where $\Phi(z) = -\beta z^2 + \ln[2 \cosh(\frac{1}{2}\beta\sqrt{\epsilon^2 + 16\bar{g}^2 z^2})]$. The form of the partition function in Eq. (64) is especially suitable for the Laplace's integral method, which consists in approximating the exponential integrand by a Gaussian function around the global maximum of the function $\Phi(z)$. By employing the Laplace approximation, one can finally obtain

$$\mathcal{Z}_{\text{DM}} \simeq \sqrt{\frac{2}{\beta\omega|\partial_z^2\Phi(z)|}} e^{N\Phi(z)} \Big|_{z=z_0}, \quad (65)$$

where z_0 is determined by $\partial_z\Phi(z)|_{z=z_0} = 0$.

With the analytical expression of the Dicke model at hand, the average value of the chosen observable \hat{J}_z can be calculate as

$$\langle \hat{J}_z \rangle = -\frac{1}{\beta} \frac{\partial}{\partial \epsilon} \ln \mathcal{Z}_{\text{DM}} = \begin{cases} -N \tanh(\beta\epsilon/2)/2, & T > T_c^{\text{DM}}; \\ -N \tanh(\beta\epsilon\eta/2)/(2\eta), & T \leq T_c^{\text{DM}}. \end{cases} \quad (66)$$

and

$$\langle \hat{J}_z^2 \rangle = \frac{1}{\beta^2 \mathcal{Z}_{\text{DM}}} \frac{\partial^2 \mathcal{Z}_{\text{DM}}}{\partial \epsilon^2} = \begin{cases} N/4 + N(N-1) \tanh(\beta\epsilon/2)/4, & T > T_c^{\text{DM}}; \\ N/4 + N(N-1) \tanh(\beta\epsilon\eta/2)/(4\eta^2), & T \leq T_c^{\text{DM}}. \end{cases} \quad (67)$$

These results recover Eq. (11) in the main text.

The universality of the T^{-1} -type scaling relation

In this section, we should provide the proof that $\partial_\epsilon^2 E_g < 0$ within the framework of the GRWA approach for the finite- N cases. Using the Feynman-Hellman theorem, one sees

$$\begin{aligned} \frac{\partial^2}{\partial \epsilon^2} E_g^{\text{GRWA}} &= \frac{\partial}{\partial \epsilon} \langle E_g^{\text{GRWA}} | \hat{J}_z | E_g^{\text{GRWA}} \rangle \\ &= \frac{\partial}{\partial \epsilon} \left\langle -\frac{N}{2}, 0 \left| e^{\lambda \hat{J}_x (\hat{a}^\dagger - \hat{a})} \hat{J}_z e^{-\lambda \hat{J}_x (\hat{a}^\dagger - \hat{a})} \right| -\frac{N}{2}, 0 \right\rangle \\ &= \frac{N}{2} \lambda e^{-\frac{1}{2}\lambda^2} \frac{\partial \lambda}{\partial \epsilon}. \end{aligned} \quad (68)$$

Together with the approximate solution of the variational parameter λ predicted by Eq. (41), one finds

$$\frac{\partial \lambda}{\partial \epsilon} = -\frac{g e^{\frac{1}{2}\lambda^2} [\epsilon g^2 + (\epsilon + \omega)^3]}{(\epsilon + \omega)^3 (\epsilon + \omega e^{\frac{1}{2}\lambda^2})^2} < 0. \quad (69)$$

Thus, we finally prove that $\partial_\epsilon^2 E_g^{\text{GRWA}} < 0$. Going beyond the GRWA treatment, we also provide the numerical evaluations of λ by using exact diagonalization method with $N = 4, 5, 6$ in Fig. 6 (b). These numerical simulations confirm our analytical predictions from the GRWA approach. The proof of $\partial_\epsilon^2 E_g < 0$ validates the universality of T^{-1} -type scaling relation in the finite- N cases, which plays a crucial role in our strategy to overcome the error-divergence problem at low temperature.

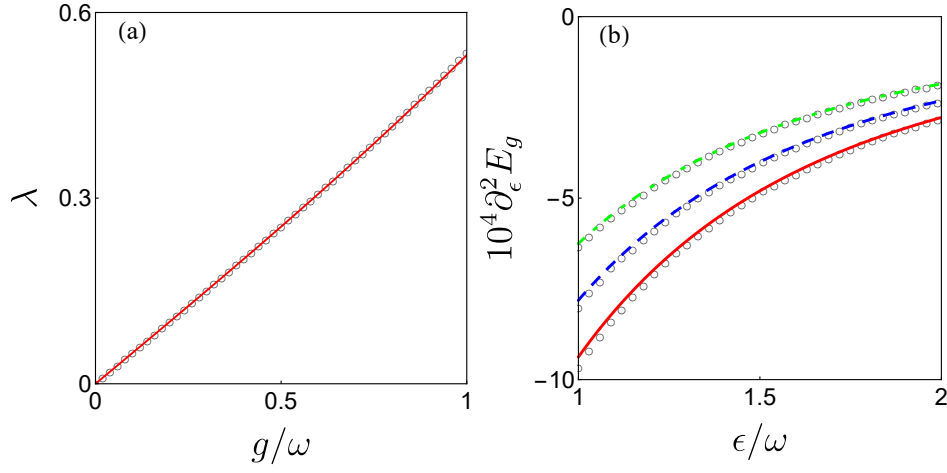


FIG. 6. (a) The variational parameter λ is plotted as a function of g/ω with $\epsilon = \omega$. The circles are the result from numerically solving the above transcendental equation Eq. (40), while the red solid line is analytical prediction by Eq. (41). (b) $\partial_\epsilon^2 E_g$ versus ϵ/ω with $g = 0.05\omega$ for different N : $N = 4$ (green dotdashed line), $N = 5$ (blue dashed line) and $N = 6$ (red solid line). The circles are numerical results from the exact diagonalization, while the lines are analytical prediction from the GRWA.

The Excitation spectrum of the Dicke model.—In this section, we would like to show that the excitation spectrum of the Dicke model becomes quasicontinuous in the limit $N \rightarrow \infty$. To this aim, we use the Holstein-Primakoff transformation [88] which represents the collective spin operators in terms of bosonic operators as follows [89]

$$\hat{J}_+ = \hat{c}^\dagger \sqrt{N - \hat{c}^\dagger \hat{c}}, \quad \hat{J}_- = \sqrt{N - \hat{c}^\dagger \hat{c}} \hat{c}, \quad \hat{J}_z = \hat{c}^\dagger \hat{c} - \frac{N}{2}, \quad (70)$$

where \hat{c} is introduced as a bosonic annihilate operator and obeys $[\hat{c}, \hat{c}^\dagger] = 1$. After the Holstein-Primakoff transformation, the Hamiltonian of the Dicke model becomes

$$\hat{\mathcal{H}}_s = \epsilon \left(\hat{c}^\dagger \hat{c} - \frac{N}{2} \right) + \omega \hat{a}^\dagger \hat{a} + \bar{g}(\hat{a}^\dagger + \hat{a}) \left(\hat{c}^\dagger \sqrt{1 - \frac{\hat{c}^\dagger \hat{c}}{N}} + \sqrt{1 - \frac{\hat{c}^\dagger \hat{c}}{N}} \hat{c} \right). \quad (71)$$

In the normal phase, one has $\hat{c}^\dagger \hat{c}/N \rightarrow 0$, which leads to

$$\hat{\mathcal{H}}_{\text{NP}} = \epsilon \hat{c}^\dagger \hat{c} + \omega \hat{a}^\dagger \hat{a} + \bar{g}(\hat{a}^\dagger + \hat{a})(\hat{c}^\dagger + \hat{c}) - \frac{1}{2} N \epsilon, \quad (72)$$

which is bilinear in terms of bosonic operators and can be diagonalized via the Bogoliubov transformation. After the Bogoliubov transformation, we have

$$\hat{\mathcal{H}}_{\text{NP}} = \sum_{\nu=\pm} \epsilon_\nu^{\text{NP}} \left(\hat{d}_\nu^\dagger \hat{d}_\nu + \frac{1}{2} \right) - \frac{1}{2} (\epsilon + \omega) - \frac{1}{2} N \epsilon, \quad (73)$$

where the excitation energies are

$$(\epsilon_\pm^{\text{NP}})^2 = \frac{1}{2} \left\{ \epsilon^2 + \omega^2 \pm \sqrt{(\epsilon^2 - \omega^2)^2 + 16\bar{g}^2 \epsilon \omega} \right\}. \quad (74)$$

In the super-radiant phase, to incorporate the effect that both the spin ensemble and the RC mode acquire macroscopic occupations, one needs to displace the bosonic modes in the way as

$$\hat{a} \rightarrow \hat{e} - \frac{N}{\omega} \sqrt{\frac{N}{4}(1 - \mu^2)}, \quad \hat{c} \rightarrow \hat{f} + \sqrt{\frac{N}{2}(1 - \mu)}, \quad (75)$$

where $\mu \equiv \epsilon\omega/(4\bar{g}^2)$. Then, the Holstein-Primakoff transformed Hamiltonian becomes

$$\begin{aligned} \hat{\mathcal{H}}_{\text{SP}} = & \omega \hat{e}^\dagger \hat{e} + \frac{\epsilon(1 + \mu)}{2\mu} \hat{f}^\dagger \hat{f} + \frac{\epsilon(1 - \mu)(3 + \mu)}{8\mu(1 + \mu)} (\hat{f} + \hat{f}^\dagger)^2 \\ & + \bar{g}\mu \sqrt{\frac{2}{1 + \mu}} (\hat{e} + \hat{e}^\dagger)(\hat{f} + \hat{f}^\dagger) - \frac{N}{2} \left(\frac{2\bar{g}^2}{\omega} + \frac{\epsilon^2 \omega}{8\bar{g}^2} \right) - \frac{\bar{g}^2}{\omega} (1 - \mu). \end{aligned} \quad (76)$$

Using the Bogoliubov transformation, the above expression can be rewritten in a diagonal form as

$$\hat{\mathcal{H}}_{\text{SP}} = \sum_{\nu=\pm} \varepsilon_{\nu}^{\text{SP}} \left(\hat{h}_{\nu}^{\dagger} \hat{h}_{\nu} + \frac{1}{2} \right) - \frac{1}{2} \left[\frac{\epsilon(1+\mu)}{2\mu} + \omega + \frac{2\bar{g}^2(1-\mu)}{\omega} \right] - \frac{N}{2} \left(\frac{2\bar{g}^2}{\omega} + \frac{\epsilon^2\omega}{8\bar{g}^2} \right), \quad (77)$$

where the excitation energies in the super-radiant phase are given by

$$(\varepsilon_{\pm}^{\text{NP}})^2 = \frac{1}{2} \frac{\epsilon^2}{\mu^2} + \omega^2 \pm \sqrt{\left(\frac{\epsilon^2}{\mu^2} - \omega^2 \right)^2 + 4\epsilon^2\omega^2}. \quad (78)$$

From these expressions, one sees that, irrespective of whether the Dicke model is in the normal phase or in the super-radiant phase, the ground-state energy E_g has the order of $O(N)$, while both the excitation energies $\varepsilon_{\nu}^{\text{NP}}$ and $\varepsilon_{\nu}^{\text{SP}}$ are $O(1)$, which leads to

$$\frac{E_e - E_g}{E_g} \simeq 1 \quad (79)$$

in the limit $N \rightarrow \infty$. This expression means the excitation spectrum of the Dicke model becomes quasicontinuous in the limit $N \rightarrow \infty$ [89] and the condition of $(E_e - E_g)/E_g \ll 1$, which is used in the analysis of the quantum Rabi model case, completely breaks down.